Received: 19 June 2019 | Revised: 1 October 2019 | Accepted: 12 October 2019

DOI: 10.1002/er.4971



RESEARCH ARTICLE

WILEY INTERNATIONAL JOURNAL OF ENERGY RESEARCH

# Experimental study on performance of square tube absorber with phase change material

**Ahmad Fadzil Sharol**[1] | **Amir Abdul Razak**[1] | **Zafri Azran Abdul Majid**[2] | **Ahmad Fudholi**[3]

[1] College of Engineering Technology, Faculty of Mechanical Engineering Technology, Universiti Malaysia Pahang, Pekan, Pahang, Malaysia

[2] Kuliyyah of Allied Health Sciences, International Islamic University of Malaysia, Kuantan, Pahang, Malaysia

[3] Solar Research Energy Institute, Universiti Kebangsaan Malaysia, Bangi, Selangor, Malaysia

**Correspondence**
Amir Abdul Razak, College of Engineering Technology, Faculty of Mechanical Engineering Technology, Universiti Malaysia Pahang, Pekan, Pahang Malaysia.
Email: amirrazak@ump.edu.my

**Funding information**
Universiti Kebangsaan Malaysia, Grant/Award Number: MRUN-RAKAN RU-2019-001/3; Universiti Malaysia Pahang, Grant/Award Number: RDU1703137

**Summary**

The intermittent nature of solar radiation has decreased the performance efficiency of solar heaters. Integrating the solar heater with thermal energy storage component could increase its performance effectively. In this article, an investigation on the effect of phase change material (PCM) as the thermal energy storage component on the performance of square aluminum tube was carried out experimentally. In the first phase, the temperature behavior of square aluminum tube with two types of PCM, namely, generic plant-based PCM (A2) and paraffin wax (A3), was compared with square aluminum tube without PCM (A1). In the second phase, the performance of square aluminum tube was investigated with different paraffin wax masses of 38 g (B1), 48 g (B2), and 58 g (B3). Based on the result, the A3 tube configuration performed better than A1 and A2 tube configurations with higher heat gain rate (0.08°C/s) and lower heat discharge rate (−0.04°C/s). The B2 tube configuration was found to have maximum heat gain of 3.73 kJ with higher heat discharge rate as compared with other square tube configurations. The average temperature difference between internal and external surface tube of B2 was lower (4.3°C) leading to higher average temperature difference at ambient temperature of 25.3°C. Instantaneous efficiency of the tube B2 is higher than the B1 and B3 tube configurations by 16% and 26%, respectively. The result suggests that the insertion of paraffin wax inside the square absorber tube improves the temperature response of the absorber in the situation of intermittent solar radiation.

**KEYWORDS**

cross-matrix absorber (CMA), phase change material (PCM), solar energy, thermal energy storage

## 1 | INTRODUCTION

Since a decade ago, fossil energy demand in the form of petroleum and coal has kept increasing every year and is expected to grow significantly for the next 50 years.[1] This annual increase of energy has raised a major concern about energy sustainability in the future. Continuous depletion of energy will cause an energy crisis that can affect global stability.[2] Heavy reliance of fossil fuels has contributed towards gradual fuel depletion as well as global warming through the release of harmful greenhouse gases thus affecting the environment and existing natural ecosystem in an adverse way.[3] Hence, alternative energy to replace these depleting sources of

  

energy is needed to avoid future energy crisis while at the same time helps to reduce the earth's environmental pollution and prevents further damage to the ecosystem.[4] Renewable energy is one of the feasible candidates of a back-up source of energy, and in recent years, it has attracted interest from the research community to create and invent suitable technologies that can harness this type of energy. Solar energy is a major source of renewable energy available in abundant quantity, and despite its low energy density characteristic and requiring a considerably large area to extract,[5] the amount of solar energy in terms of annual solar radiation that reaches the surface of earth is much greater than the combined amount of all nonrenewable energy sources.[6] Even so, technologies related to solar energy always suffer from ineffective performance of the device itself during application. This is due to the intermittent nature of the sun's radiation that limits the utilization of solar-heated device during night time or during off-sunshine hours and hence preventing it from reaching its true potentials.

In order to address the issue, utilization of a device coupled with thermal storage system has been considered in order to extend useful operating hours of the solar energy systems.[7] Research and development of integration of solar air heater with thermal energy storage material have become the main focus in the field of solar engineering technology. Methods of storing thermal energy including sensible heat and latent heat have been employed. The method of latent heat with the application of phase change material (PCM) has received a special attention because of its higher energy storage density compared with sensible heat energy storage material.[8,9] It works on the principle where the material itself will store and release an amount of heat when the phase changes during the operation.[10,11] A review study of thermal energy storage integration with solar heaters has been conducted by Haldorai et al.[12] From the study, it is concluded that solar heaters with latent heat energy storage material as a thermal energy storage component provide a better thermal efficiency when compared with solar heaters employing other types of thermal energy storage materials. Many solar air heater applications using latent heat energy storage materials such as hydrated salt,[13] palmitic and lauric acid,[14,15] and technical grade paraffin wax[11,12] have been studied. These applications include space heating/cooling,[16] food packaging,[17] and water desalination system.[18]

Among these types of PCM, technical grade paraffin wax is the most popular PCM used for latent heat energy storage material in solar air heater applications[19] because of its ability to provide a wide range of application temperature, less expensive, chemically stable, and suitable to be used in many types of metal container.[9,15]

In terms of absorber geometry selection of the container, various designs have been studied by previous researchers such as flat plate with extended surface[20] and packed bed.[21,22–23] Fath[22] conducted a simulation to study a simple integrated solar air heater with variations of PCM as thermal energy storage inside a cylinder tube with different tube arrangements. Based on the study, paraffin wax performed better with 63.35% at 0.02 kg/s with zig-zag cylinder tube arrangement across an airflow direction. An experiment of integrated flat plate solar air heater was conducted by Enibe[24] in which paraffin wax was used as PCM material inside a slender square module as PCM container. Under natural air circulation, maximum outlet temperature of the air heater was 60°C with 50% efficiency. El-Khadraoui et al[25] conducted an experimental comparison of integrated solar air heater where the sizing of the PCM-filled cavity was presented with the PCM mass determined using thermal energy balance during the charging phase. Based on the result, they found that the solar air heater with PCM was able to maintain a higher output temperature difference with an efficiency of 17% higher than the one without PCM. The effect of mass flow rate and the mass of PCM on the performance of an integrated solar air heater with finned plate absorber was investigated by Kabeel et al.[23] The experimental result showed that the heavier the PCM mass, the longer operation hours of the solar air heater can be achieved after sunset. The daily efficiency of the heater with PCM is higher than the one without PCM by 10.8% to 13.6%.

A work done by AA Razak[26] focused on the development of a single pass cross-matrix absorber (CMA) for air-based solar collector. In the work, the combination of different materials of square tube, namely, stainless steel and aluminum, was used as the thermal absorber for the collector. The stainless-steel square tube was used to create the thermal buffer in order to stabilize the output temperature. However, the heavier fluctuation of solar radiation will affect the overall performance of the collector because of the lower thermal diffusivity of the thick stainless-steel tubes.[27] Based on the authors' knowledge, there have been no studies with regard to the integration of matrix absorber with PCM materials reported in the literature. The main objective of this work is therefore to investigate the thermal characteristics of square aluminum tubes using PCM as the thermal energy storage materials. The performance comparison between generic plant-based PCM and paraffin wax was conducted. Additionally, the performance of the square aluminum tube based on paraffin wax's mass variation of 38, 48, and 58 g was conducted.

## 2 | DEVICE AND APPARATUS

The experimental devices and apparatus used in this work are explained in this section. A solar simulator (consisting of nine units of 150-W halogen lamp) was used to provide an artificial solar simulation into square tube absorbers that are capable of producing maximum solar radiation flux of 1350 W/m$^2$. In order to determine the average artificial solar radiation of 900 W/m$^2$, the perpendicular distance between the solar simulator's halogen lamp and the square tubes wax was fixed at 455 mm. Artificial solar radiation produced by the solar simulator was measured using a pyranometer (model number SP-110-SS by Apogee Instrument, USA). Additionally, the temperature data were measured using six units of k-type thermocouple and three units of digital temperature sensor. Table 1 details out the accuracy of the measuring instrument used in this work. The containment acts as a miniabsorber comprising aluminum square tubes (with dimensions of 2-cm height × 2-cm width × 40-cm length) sprayed with flat black coating system. In order to avoid heat losses through the bottom and sides of the containment, a 4-mm thickness of insulation layer was applied.

### 2.1 | Uncertainty analysis

The uncertainties of the collected data measured by experimental devices explained in Section 2 are elaborated in this section. Table 2 shows the uncertainties of evaluation of the parameters used in this study. The uncertainties measurement from Moffat[28] and Yahya et al[29] have been adopted in this work. For $x_n$ number of measurements made, each has a measurement tolerance of $\sigma_n$, and the uncertainty of the measurement parameters, $U_R$, can be calculated using the following formula:

$$U_R = \sqrt{\left(\frac{U_R}{dx_1}.\sigma_1\right)^2 + \left(\frac{U_R}{dx_2}.\sigma_2\right)^2 + \left(\frac{U_R}{dx_3}.\sigma_3\right)^2 + \ldots\left(\frac{U_R}{dx_n}.\sigma_n\right)^2}. \quad (2.1)$$

The uncertainty and relative uncertainty of the heat gained by the square aluminum tube are 0.421 × 10$^{-3}$ kJ and 3.2%, respectively, as obtained from Equation 2.1.

**TABLE 1** Accuracy of measuring instruments used in this work

| Measuring Instrument | Quantity | Accuracy |
|---|---|---|
| K-type thermocouple | 6 | −1.5°C to +1.5°C |
| Digital temperature sensor | 3 | −1.0°C to +1.0°C |
| Pyranometer | 1 | 0.1 W/m$^2$ |

**TABLE 2** Uncertainty of the important parameters involved in this work

| Description | Unit | Uncertainty | Relative Uncertainty, % |
|---|---|---|---|
| Outer temperature | °C | ±0.10 | 0.48 |
| Internal temperature | °C | ±0.15 | 0.72 |
| Ambient temperature | °C | ±0.10 | 0.48 |
| Solar radiation | W/m$^2$ | ±12 | 2.04 |

## 3 | METHODOLOGY

All experimental works have been conducted in the laboratory under a controlled environment. The details of each experiment conducted are explained in the following sections.

### 3.1 | Measurement of melting and solidification temperature of generic plant-based PCM

One of the PCMs used in this study was a generic plant-based PCM in a solid form manufactured by Ikea. In this section, the determination of melting and solidification for generic plant-based PCM was conducted, and the experimental setup including sensor locations is shown in Figure 1. Three units of digital temperature sensor were used to record the temperature data, namely, T1, T2, and T3. T1 was used to sense the temperature of PCM, while T2 and T3 were used to sense the water and ambient temperature, respectively. The 1000-W hot plate was used to increase the water temperature until the heat transfer occurred in order to increase the temperature of the PCM material (generic plant-based PCM). The water was stirred every 15 minutes in order to stabilize the heat distribution around the PCM until the wax form was in liquid phase at temperature of 90°C (Figure 1A). Additionally, a small support made from a nonheat conductor material was used to support the bottom containment of the PCM. This was followed by removing the heat source through placing the assembly in ambient condition in order to replicate the cooling process (Figure 1B). During the cooling process, the temperature readings from all sensors were manually recorded every 10-minute time span for 3 hours of the cooling process. Figure 2 presents the variation of PCM drop temperature. As can be seen, the temperature rapidly drops during the first 20 minutes and then further dropped gradually before it became constant at around 42°C to 43°C. It is shown that the solidification temperature of PCM

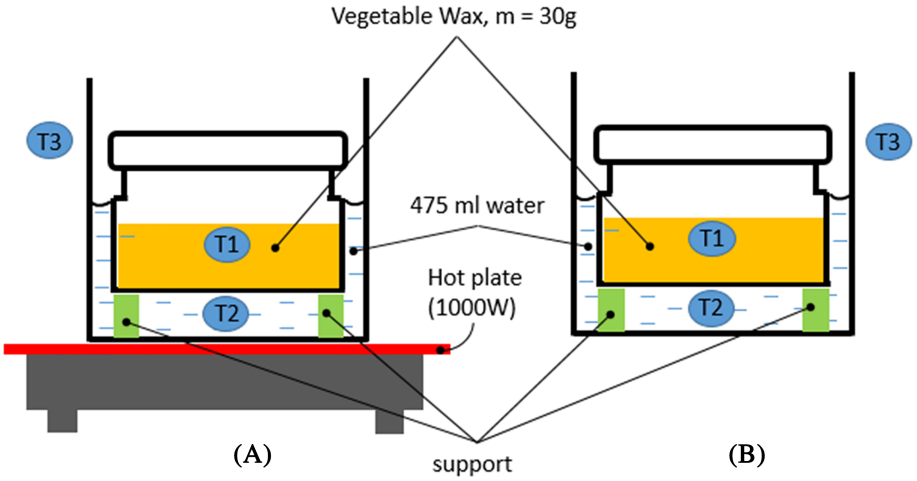


**FIGURE 1** Experimental setup for determining the melting-solidification temperature of generic plant-based PCM: (A) heating and (B) cooling [Colour figure can be viewed at wileyonlinelibrary.com]

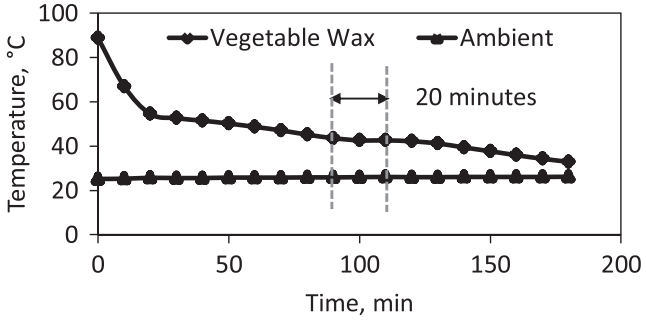


**FIGURE 2** Variation of solidification temperature of generic plant-based PCM during cooling process

(generic plant-based PCM) is around 42°C to 43°C, in which latent heat of fusion being released from the system to the environment occurs for about 20 minutes before it further solidifies until its temperature approaches to ambient temperature value.[30] Additionally, paraffin wax has been used as the second PCM in order to evaluate the thermal performance of the square tube used in this work. The thermophysical properties of paraffin wax is shown in Table 3.

**TABLE 3** Thermophysical properties of paraffin wax used in this work[31,32]

| Thermophysical Properties | Unit | Values |
|---|---|---|
| Melting temperature | °C | 58-60 |
| Specific heat | kJ/kg K | 0.9 |
| Enthalpy of fusion | kJ/kg | 214.4 |
| Thermal conductivity | W/m K | 0.2 |
| Solid density | kg/m$^3$ | 850 |
| Liquid density | kg/m$^3$ | 775 |

## 3.2 | Experimental procedure

The experimental works in this study were conducted in two phases with the setup for both phases shown in Figure 3. The overall process flow chart of the experimental works and details of the absorber configuration are shown in Figure 4 and Table 4, respectively. The first phase involves experimental comparison of thermal storage capability of A1, A2, and A3 tube configurations. Under the condition of no air flow (v = 0 m/s), the tubes were exposed to artificial solar radiation of 900 W/m$^2$ for 30 minutes to simulate the charging process. The temperature data were collected and recorded at every 10

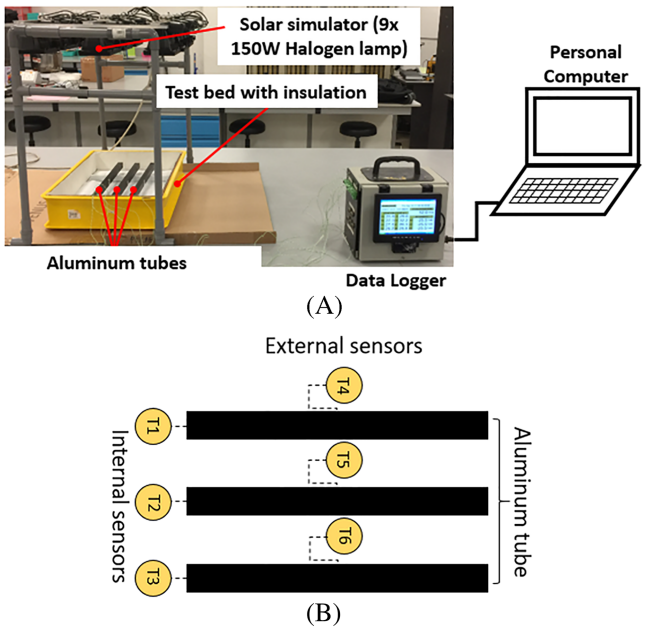


**FIGURE 3** (A) Experimental setup and (B) temperature sensor location [Colour figure can be viewed at wileyonlinelibrary.com]

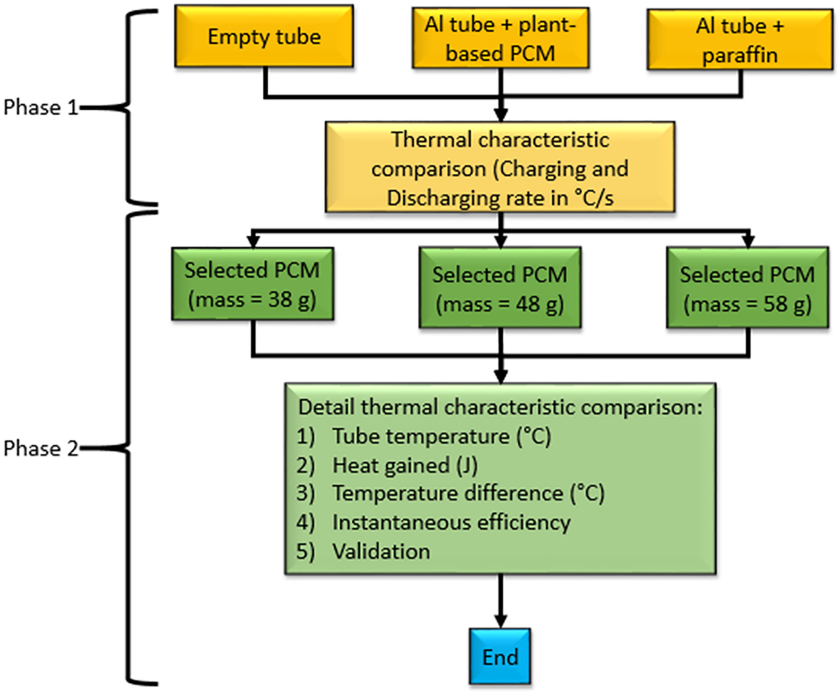


**FIGURE 4** Process flow chart implemented in this work [Colour figure can be viewed at wileyonlinelibrary.com]

**TABLE 4** Detailed thermal absorber configuration used in each phase of experimental work

| Thermal Absorber Configuration | Representation |
|---|---|
| Phase 1 | |
| Hollow square aluminum tube | A1 |
| Plant-based PCM-filled square aluminum tube | A2 |
| Paraffin wax–filled square aluminum tube | A3 |
| Phase 2 | |
| Square aluminum tube with 38 g selected PCM | B1 |
| Square aluminum tube with 48 g selected PCM | B2 |
| Square aluminum tube with 58 g selected PCM | B3 |

seconds using a data logger. Temperature sensors T1, T2, and T3 were used to record the internal tube temperatures containing the PCM, while T4, T5, and T6 were used to record the external tube temperatures. The discharge process was conducted by removing the solar simulator and the process continued for another 30 minutes. Similar procedure of collecting and recording the data was implemented. Then the selection of PCM material for the next phase of experiment was made based on the performance of each square tube configuration from phase one experiment. The second-phase experiment involved determining the effect of PCM mass (selected from phase one experiment) with mass variation of 38, 48, and 58 g in order to investigate the performance and heat storage capability of each configuration. The mass was made to have 10-g difference to each other, and this mass value was limited to the size capacity of the square aluminum tube used in this experiment. Similar procedure of collecting and recording the temperature data was adapted in phase two experimental work.

### 3.3 | Experimental comparison

In order to confirm the effectiveness of the PCM inside the square aluminum tube of CMA, an experimental comparison was carried out with the previous work done by Majid et al.[3] The work method was replicated based on the tube arrangement, temperature measurement procedure, and simulated solar radiation of 590 W/m$^2$ and was performed under a control environment. The outcome of the experiment would focus on the discussion related to output temperature profile and heat discharge rate during the final 15 minutes of the charging process and will be presented in the latter sections.

## 4 | RESULTS AND DISCUSSION

### 4.1 | Comparison study between square hollow aluminum tube (A1), generic plant-based PCM-filled square aluminum tube (A2), and paraffin wax–filled square aluminum tube (A3)

In order to understand the heat transfer mechanism and heat storage capability of PCM inside the square aluminum tubes, three aluminum tubes with different configurations

of A1, A2, and A3 were exposed in an artificial solar radiation for about 30 minutes to simulate charging process and a further 30 minutes to simulate the discharging process when the artificial solar radiation was removed. The experimental results are presented in Figure 5 showing the temperature behavior of these tubes taken from an external sensor. It can be seen clearly in the figure that, during the initial stage of charging period, the temperature of A1 tube configuration was rapidly increasing. At $t = 500$ seconds, the rate started to reduce and achieve maximum temperature of 99°C at $t = 1810$ seconds. This was expected because of the fact that aluminum is a good thermal diffuser[27,33] causing heat distribution throughout the entire tube section occurring in a short period of time. In contrast, the temperature rise rate for A2 and A3 tube configurations occurs at a slow rate and achieve maximum temperature of 92.7°C and 93.8°C, respectively.

With the assumption of constant mass and heat capacity of the square aluminum tube and paraffin wax, the rate of heat charge and discharge was calculated based on the following equations:

$$\text{Heat Charging rate} = \frac{\Delta T_{Ch}}{\Delta t_{Ch}}, \tag{4.1}$$

$$\text{Heat Discharging rate} = \frac{\Delta T_{Dis}}{\Delta t_{Dis}}, \tag{4.2}$$

where $\Delta T_{Ch}$, $\Delta T_{Dis}$, $\Delta t_{Ch}$, and $\Delta t_{Dis}$ are temperature differences and times during charging and discharging period, respectively. In the course of the discharging period, the temperature drop of A1 tube configuration was slightly faster than the other two tube configurations. The calculated heat discharging rate for aluminum was −0.11°C/s as compared with −0.05°C/s and −0.04°C/s for A2 and A3 tube configurations, respectively. Heat discharging rate for A1 tube configuration experienced the highest rate of heat release of −0.17°C/s at $t = 1930$ seconds. The negative sign means heat release from the systems, in which the rate of heat release by A3 tube configuration is slightly slower than the one by A2 tube configuration.[30] This indicates that A3 tube configuration promotes higher heat storage capability because of its characteristic to retain the same amount of heat in a prolonged time compared with the A2 tube configuration. Based on this result, the paraffin wax was selected as a PCM material to be used in the next phase of experiment. Table 5 summarizes the heat charging rate and heat discharge rate of each square aluminum tube configuration.

## 4.2 | Influence of PCM to the square aluminum tube absorber (B1, B2, and B3)

In order to study the effect of PCM mass (in this case, paraffin wax) on the temperature behavior of the square aluminum tube, similar experimental procedures used in the first-phase experiment are adopted here. Figure 6 shows the temperature behavior of paraffin wax–filled square aluminum tube with different mass values. As clearly seen, in the charging period, the temperature of B1 tube configuration increases slightly faster than the other two square aluminum tube configurations. This behavior is expected as the amount of energy required from the heat supplied to the square aluminum tube to melt the PCM is

**TABLE 5** Summary of heat charging and heat discharging rates of different square aluminum tube configurations

| Square Aluminum Tube Configuration | Heat Charging Rate, °C/s | Heat Discharging Rate, °C/s | Maximum Temperature, °C |
|---|---|---|---|
| A1 | 0.14 | -0.11 | 99.3 |
| A2 | 0.07 | -0.05 | 92.7 |
| A3 | 0.08 | -0.04 | 93.8 |

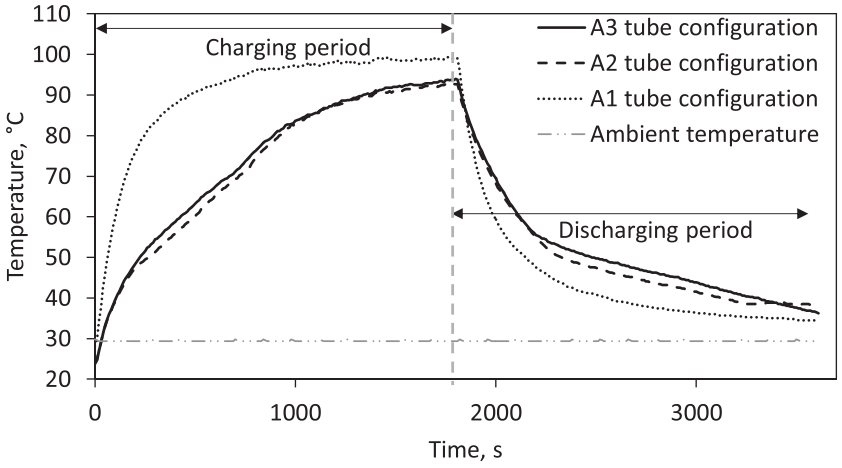


**FIGURE 5** Temperature behavior of different square aluminum tube configurations: hollow, generic plant-based PCM-filled and paraffin wax-filled square aluminum tubes

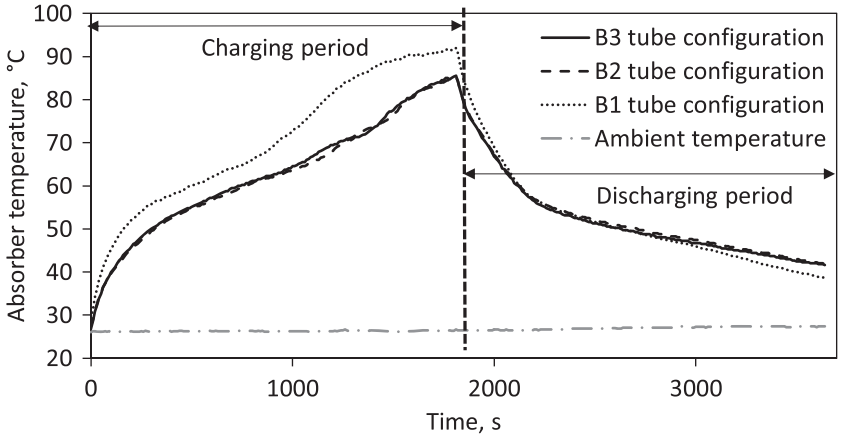


**FIGURE 6** Temperature behavior of square aluminum tube based on different masses of paraffin wax

less, as compared with the other two square aluminum tube configurations. At $t = 1800$ seconds, the maximum temperature was achieved by each tube configuration (91.5°C, 85°C, and 85.4°C for B1, B2, and B3 tube configurations, respectively).

During the discharging period, all configurations of square aluminum tubes experienced fairly the same heat discharge rate until $t = 2780$ seconds in which the temperature drop behavior was slightly faster for B1 tube as compared with B2 and B3 tubes. The heat discharging rate for B1 tube was −0.02°C/s as compared with B2 and B3 tube configurations of −0.01°C/s (both having the same value). The summary of heat charging and discharging rate of each square aluminum tube configuration is presented in Table 6. The negative sign in the heat discharging rate value means heat being released from the systems.

## 4.3 | Thermal analysis of B1, B2, and B3 absorbers

In order to evaluate the performance of each configuration of square aluminum tube with paraffin wax, a thermal analysis was performed to determine each configuration capability in terms of gaining and storing the energy. The study conducted by Majid et al[3] shows that square aluminum tube alone tends to increase and reduce its temperature faster making it unsuitable for storage purposes. For assumption, the system in this study was considered as a closed system and did not involve any velocity and elevation change. Hence, the square tube absorber's energy variation during the charging and discharging period is expressed as follows[30]:

$$Q_{g,Al} = m_{Al} c_{Al} \left(T_f - T_i\right), \tag{4.3}$$

while energy variation stored by the PCM is expressed as follows[23]:

$$\mathrm{Q_S} = \frac{\mathrm{m_{pcm}}}{\Delta \mathrm{t}} \mathrm{c_{p,s}} \Delta \mathrm{T_{pcm}} \quad \mathrm{T_{avg,pcm}} < \mathrm{T_m},$$

$$Q_S = \left(\frac{m_{pcm} l_{pcm}}{\Delta t}\right) T_{avg,pcm} = T_m, \tag{4.4}$$

$$\mathrm{Q_S} = \frac{\mathrm{m_{pcm}}}{\Delta \mathrm{t}} \mathrm{c_{p,l}} \Delta \mathrm{T_{pcm}} \; \mathrm{T_{avg,pcm}} > \mathrm{T_m},$$

where $Q_{g,Al}$ is the heat gain by the square aluminum tube (kJ), $m_{Al}$ is the mass of aluminum (kg), $m_{pcm}$ is the mass of PCM (kg), $c_{Al}$ is the specific heat of aluminum (kJ/kg °C), $c_{p,s}$ is the specific heat of PCM (solid state) (kJ/kg °C), $l_{pcm}$ is the latent heat of PCM (kJ/kg), $T_{pcm}$ is the temperature of PCM (°C), and $T_m$ is the melting temperature (°C). With the no-flow condition (air mass flowrate, $\dot{m} = 0$), the total useful energy gained by the system can be calculated as the sum of energy gain by both absorber tube and the PCM as follows:

$$Q_u = Q_{g,Al} + Q_S. \tag{4.5}$$

The charging and discharging instantaneous efficiencies of the process are calculated using the following Equations (4.6) and (4.7)[23,34]:

**TABLE 6** Summary of heat gain and heat discharge rate of square aluminum tube with different paraffin wax's masses

| Square Aluminum Tube Configuration | Heat Charging Rate, °C/s | Heat Discharging Rate, °C/s | Maximum Tube Temperature, °C |
|---|---|---|---|
| B1 | 0.05 | −0.02 | 92 |
| B2 | 0.02 | −0.01 | 85.2 |
| B3 | 0.03 | −0.01 | 85.6 |

$$\eta = \frac{Q_U}{IA_C}, \tag{4.6}$$

$$\eta = \frac{Q_U}{Q_S}, \tag{4.7}$$

where $Q_u$ and $Q_L$ are total useful energy and latent heat energy by the system in J, respectively, while $I$ and $A_C$ are solar radiation (W/m$^2$) and aperture area of the tube (m$^2$), respectively.

The variation of heat gain by the square aluminum tube is presented in Figure 7. During the first 5 minutes of the charging period, the heat gain by B1 tube configuration is faster than the other two configurations (B2 and B3). This observation is expected as the heat received by the square aluminum tube was less used to melt the paraffin wax. Unlike B1 tube configuration, B2 and B3 tube configurations experienced slower heat gains because of the heat supplied being used to melt the considerably large amount of paraffin wax. Maximum heat attained by the B1 tube was 4.04 kJ while for B2 and B3 was 3.73 and 3.77 kJ, respectively. We can conclude that for B1 tube, the time taken for paraffin wax to completely melt is faster than the other two configurations. This was the main contribution of B1 tube achieving maximum tube temperature during the charging period.

The heat transfer variation during discharging period for all square tubes is illustrated in Figure 8. The B1 tube configuration experiences the highest heat discharge rate among all aluminum tube configurations. Within 5 minutes of the discharging process, the heat content from B1 tube already reaches 2 kJ. This behavior is expected as the lesser amount of paraffin wax requires shorter solidification time, hence the heat released by the system occurring in a shorter period.

Meanwhile, B3 tube configurations undergoing almost similar heat discharge rate with the B2 tube configuration

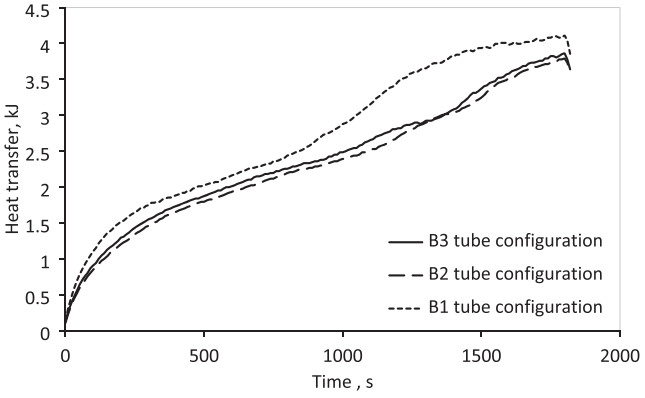


**FIGURE 7** Variation of heat transfer based on different square aluminum tube configurations (B1, B2, and B3) during charging period

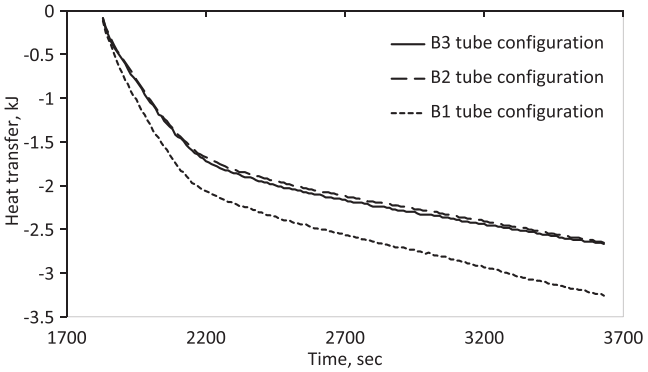


**FIGURE 8** Variation of heat transfer on different square aluminum tube configurations (B1, B2, and B3) during discharge period

exhibit a slightly lower heat discharge rate as shown in Figure 8. This was probably due to the uneven heat distribution for B3 tube configuration. During the discharging period, as the thickness layer of the paraffin wax increases, we can conclude that the heat stored in the B3 tube configuration was not able to completely melt the paraffin wax as a result of low thermal conductivity of the paraffin wax.[35] Instead, the heat supplied to the B3 tube configuration was dissipated to the environment through the internal wall of aluminum tube and upper surface of the paraffin wax.[36] While for B2 tube configuration, almost all heat stored by the paraffin was used to heat up the aluminum internal wall, leading to the high-temperature profile. It is concluded that the mass value of 48 g was the optimum mass value of paraffin wax to be used in the square aluminum tube for CMA design.

The difference between external and internal temperature readings of each square aluminum tube configuration is presented in Figure 9. During the starting of discharging period at $t$ = 1820 seconds, each square aluminum tube configuration experiences higher temperature inside the tube. Most notably, for B2 tube

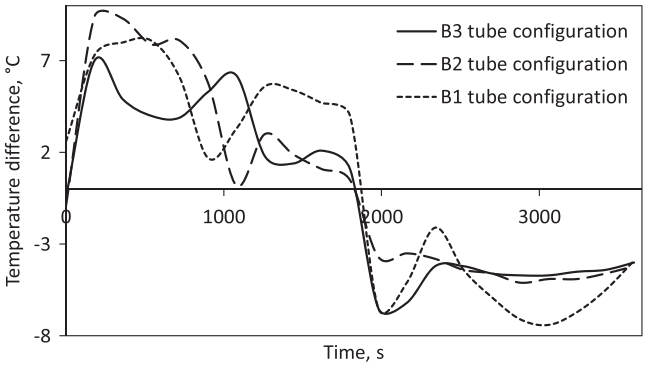


**FIGURE 9** Temperature difference between external and internal temperature sensors of each square aluminum tube configuration

configuration, the average internal and external surface temperature difference was 4.3°C, as summarized by Table 7.

In order to evaluate the performance of each tube in terms of heat storage capability, instantaneous efficiency of the tube during the discharging process was calculated using Equation (4.3), and the results are compared and presented in Figure 10. The discharging instantaneous efficiency of all tubes are evaluated, for instance at $t$ = 2220 seconds. The B2 tube configuration's instantaneous discharging efficiency was 69%, which is the highest among the other two tube configurations of 53% and 43% for B1 and B3 tube configurations, respectively. In terms of temperature difference between the tube and ambient temperature at that specific time, B1 and B3 tube configurations achieved the same temperature difference of 30°C, which is almost 1°C higher than that of B3 tube configuration. As can be seen in Figure 8, B2 tube configuration discharge rate is the slowest among the other tubes. This shows that B2 tube configuration is able to retain the temperature difference with an ambient temperature at a prolonged time and improves the tube performance as a thermal absorber component during fluctuations of the solar radiation. A potential significant improvement is expected when the number of tube increases.

**TABLE 7** Summary of average temperature difference between internal and external as well as between external surface ($T_s$) and ambient temperature ($T_a$)

| Square Aluminum Tube Configuration | Average Temperature Difference, °C | Average $T_s - T_a$, °C |
|---|---|---|
| B1 | 5.3 | 24.5 |
| B2 | 4.3 | 25.3 |
| B3 | 4.8 | 24.7 |

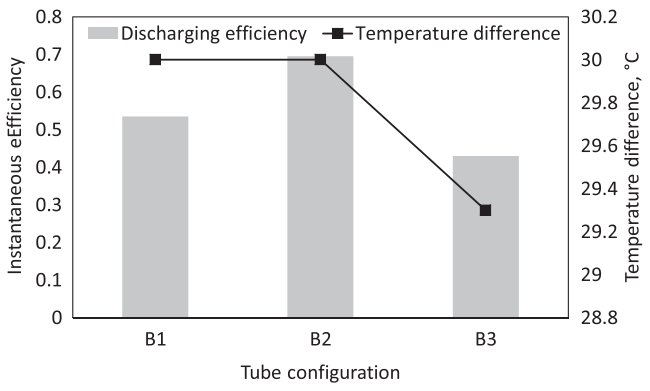


**FIGURE 10** Instantaneous efficiency-external temperature mapping of square aluminum tube with paraffin wax mass of (a) B3, (b) B2, and (c) B1 tube configurations

## 4.4 | Experimental comparison results

The output temperature profile of the experimental comparison is presented in Figure 11. During the beginning until the end of the charging process, at $t$ = 15 minutes, the charging rate of square aluminum tube without PCM achieves the highest rate among the other square tube configurations. This behavior is expected because of the higher thermal diffusivity possessed by aluminum tube.[37] As for square aluminum tube with PCM, the temperature increment during the charging process is slightly lower than both hollow tubes because of the fact that the heat received by the tube was used to melt the PCM. However, these thermophysical properties were not significant in retaining the heat during the discharging process as the hollow aluminum tube experienced the fastest temperature drop. In contrast, for the aluminum tube with PCM, the temperature drop occurred at a slower rate compared with other tube configurations. The square aluminum tube with PCM performed better compared with the square stainless-steel tube with PCM in terms of ability to achieve higher temperature during charging and retaining the temperature during the discharging period.

Figure 12 presents the discharging rate of each tube configuration according to its respective temperature profiles. Based on the plotted figure, it is found that hollow square aluminum tube experiences a rapid discharging rate of around −0.1°C/s during the first 5 minutes of discharging process. As compared with discharging rate at the first 5 minutes for other tube configuration, hollow square stainless steel, square stainless steel with PCM, and square aluminum with PCM tube discharging rate are 0.07°C/s, 0.01°C/s, and 0.02°C/s, respectively. As the discharging process goes further down, the discharging rate of each tube occurs at almost similar rate, but tubes with PCM are 6.2°C

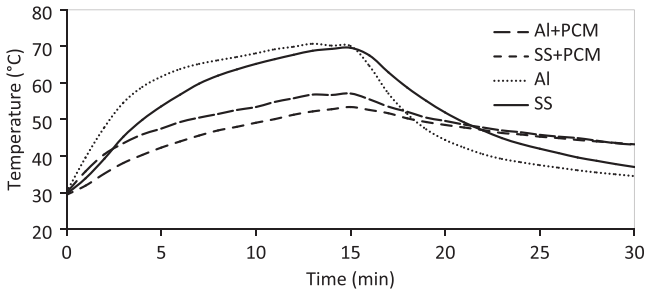


**FIGURE 11** Temperature profile of each square tube absorber based on material

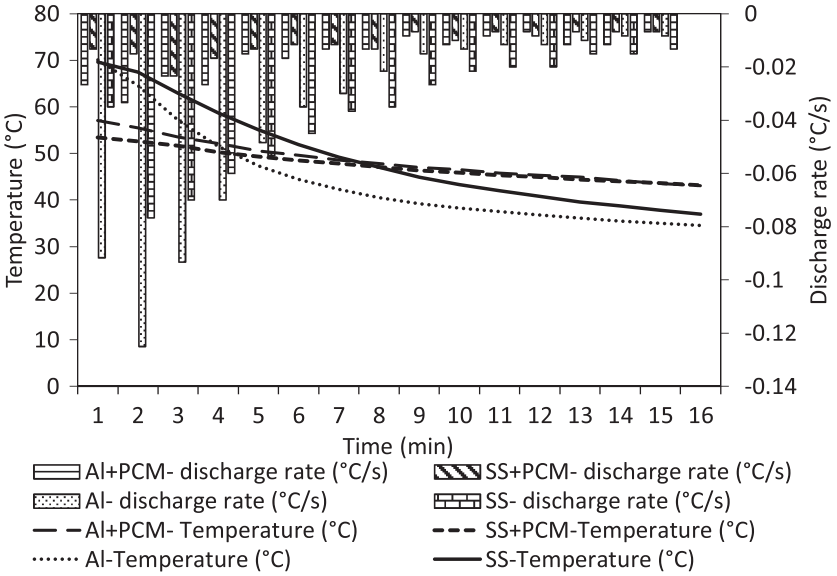


**FIGURE 12** Temperature profile and discharge rate of each square tube configuration during discharging process

higher than the tube without PCM. This validated result shows that tubes with PCM perform better in terms of retaining heat and are therefore useful in solar air.

## 5 | CONCLUSION

The effects of temperature, energy gain, and storage capability of square aluminum tubes were studied in this work. Several square aluminum tubes with different PCM materials were constructed to investigate their performance by determining their heat charging and discharging rate. Based on the results, paraffin wax was chosen as a PCM material to be integrated with the square aluminum tubes, and their performance was investigated based on a variation of mass values. Based on this experimental work, several conclusions are made as follows:

- Paraffin wax performed slightly better than the generic plant-based PCM with the earlier providing high heat charging rate of 0.08°C/s and low heat discharge rate of −0.04°C/s with 63% and 20% slower than those of hollow tube and generic plant-based PCM-filled tube, respectively.
- Forty-eight-gram mass of paraffin wax was the optimum value to be used with square aluminum tube with dimensions of $(2 \times 2 \times 40)$ $cm^3$.
- Low thermal conductivity of the paraffin wax leads to an ineffective heat distribution across paraffin of B3 aluminum tube configuration; this is due to the increment of paraffin wax thickness layer, causing the heat dissipated into the environment through the upper layer of the paraffin wax and internal wall of the aluminum tube before it can melt the remaining of the paraffin wax inside the tube configuration.
- There is a potential of having a high energy gain and high heat storage capacity when the PCM–square aluminum tube configuration to be used in CMA as the CMA-PCM air heater.
- The thermal absorbers with this feature (PCM integrated inside absorber tube) lead to compact and space saving collector system with several advantages such as cost saving for additional insulation material for PCM containment and also require no additional spaces as the PCM was inserted inside the existing structures (aluminum tube absorber).
- The experimental validation has been fully carried out. It was shown that tubes with PCM performed better in terms of heat retaining capability as compared with the tube without PCM.

## ACKNOWLEDGEMENTS

The authors wish to express their grateful acknowledgement to Universiti Malaysia Pahang for the financial support under project grant RDU1703137 and Universiti Kebangsaan Malaysia under project grant MRUNRAKAN RU-2019-001/3.

## ORCID

*Ahmad Fadzil Sharol* https://orcid.org/0000-0001-8082-9369
*Amir Abdul Razak* https://orcid.org/0000-0001-5479-7025
*Ahmad Fudholi* https://orcid.org/0000-0002-9528-7344

## REFERENCES

1. Kalogirou S. *Solar Energy Engineering: Processes and Systems*. Elsevier Inc.; 2009.

2. Razak AA, Majid ZAA, Azmi WH, et al. Review on matrix thermal absorber designs for solar air collector. *Renew. Sustain. Energy Rev.* 2016;64:682-693.
3. Majid ZAA, Razak AA, Ruslan MH, Sopian K. Characteristics of solar thermal absorber materials for cross absorber design in solar air collector. *Int. J. Automot. Mech. Eng.* 2015;11(1):2582-2590.
4. Al-Zareer M, Dincer I, Rosen MA. A novel phase change based cooling system for prismatic lithium ion batteries. *Int. J. Refrig.* 2018;86:203-217.
5. Alam T. and Kim M. H., "A critical review on artificial roughness provided in rectangular solar air heater duct," *Renew. Sustain. Energy Rev.*, vol. 69, no. July 2016, pp. 387–400, 2017.
6. Thirugnanasambandam M, Iniyan S, Goic R. A review of solar thermal technologies §. *Renew. Sustain. Energy Rev.* 2010;14:312-322.
7. Khan M. M. A., Ibrahim N. I., Mahbubul I. M., Muhammad H.. Ali H.M, Saidur R., and Al-Sulaiman F. A., "Evaluation of solar collector designs with integrated latent heat thermal energy storage: A review," *Sol. Energy*, vol. 166, no. April, pp. 334–350, 2018.
8. Farid MM, Khudhair AM, Razack SAK, Al-Hallaj S. A review on phase change energy storage: Materials and applications. *Energy Convers. Manag.* 2004;45(9–10):1597-1615.
9. Sharma A, Tyagi VV, Chen CR, Buddhi D. Review on thermal energy storage with phase change materials and applications. *Renew. Sustain. Energy Rev.* 2009;13(2):318-345.
10. Sevinchan E, Dincer I, Lang H. Investigation of heat transfer performance of various insulating materials for robots. *Int. J. Heat Mass Transf.* 2019;131:907-919.
11. Omara A. A. M. and Abuelnour A. A. A., "Improving the performance of air conditioning systems by using phase change materials: A review," *Int. J. Energy Res.*, no. December 2018, pp. 1–24, 2019.
12. Haldorai S., Gurusamy S., and Pradhapraj M., "A review on thermal energy storage systems in solar air heaters," *Int. J. Energy Res.*, no. June 2018, pp. 1–17, 2019.
13. Myers PD, Bhardwaj A, Goswami DY, Stefanakos E. Chloride Salt Systems for High Temperature Thermal Energy Storage: Properties and Applications. *Vol. 1 Adv. Sol. Build. Conserv. Clim. Control Environ. Altern. Fuels Infrastructure; ARPA-E; Comb. Energy Cycles, CHP, CCHP, Smart Grids; Conc. Sol. Power; Econ. Environ. Policy Asp*. 2015;V001T03A003.
14. Hasan A. Phase change material energy storage system employing palmitic acid. *Sol. Energy*. 1994;52(2):143-154.
15. Alain Joseph MAW, Kabbara M, Groulx D, Allred P. Characterization and real-time testing of phase-change materials for solar thermal energy storage. *Int. J. energy Res.* 2015.
16. Chinnasamy V, Appukuttan S. A real-time experimental investigation of building integrated thermal energy storage with air-conditioning system for indoor temperature regulation. *Energy Storage*. 2019;1(3):e43.
17. Ünal M., Konuklu Y., and Paksoy H., "Thermal buffering effect of a packaging design with microencapsulated phase change material," *Int. J. Energy Res.*, no. April, pp. 1–11, 2019.
18. Demir ME, Dincer I. Development and analysis of a new integrated solar energy system with thermal storage for fresh water and power production. *Int. J. Energy Res.* 2018;42(9):2864-2874.
19. Yousef M. S., Hassan H., Kodama S., and Sekiguchi H., "An experimental study on the performance of single slope solar still integrated with a PCM-based pin-finned heat sink," *Energy Procedia*, vol. 156, no. September 2018, pp. 100–104, 2019.
20. Ghiami A, Ghiami S. Comparative study based on energy and exergy analyses of a baffled solar air heater with latent storage collector. *Appl. Therm. Eng.* 2018;133:797-808.
21. Bouadila S, Kooli S, Lazaar M, Skouri S, Farhat A. Performance of a new solar air heater with packed-bed latent storage energy for nocturnal use. *Appl. Energy*. 2013;110:267-275.
22. Hassan ES, Fath HE. Thermal performance of a simple design solar air heater with built-in thermal energy storage system. *Renew. Energy*. 1995;6(8):1033-1039.
23. Kabeel AE, Khalil A, Shalaby SM, Zayed ME. Improvement of thermal performance of the finned plate solar air heater by using latent heat thermal storage. *Appl. Therm. Eng.* 2017;123:546-553.
24. Enibe SO. Performance of a natural circulation solar air heating system with phase change material energy storage. *Renew. Energy*. 2002;27(1):69-86.
25. El Khadraoui A, Bouadila S, Kooli S, Guizani A, Farhat A. Solar air heater with phase change material: An energy analysis and a comparative study. *Appl. Therm. Eng.* 2016;107:1057-1064.
26. Razak AA. Performance of Bi-Metallic Cross Matrix Absorber in Air Based Solar Air Collector. *PhD Thesis, Univ. Kebangs. Malaysia*. 2017.
27. Razak AA, Majid ZAA, Ruslan MH, Sopian K. Thermal absorber material selection for solar thermal Bi-Metallic multilayer crosses absorber. *Int. J. Adv. Appl. Sci.* 2016;3(8):57-60.
28. Moffat R. J., "Contributions to the Theory of Single-Sample Uncertainity Analysis," *J. Fluids Eng.*, vol. 104, no. June, pp. 250–258, 1982.
29. Yahya M, Fudholi A, Sopian K. Energy and exergy analyses of solar-assisted fluidized bed drying integrated with biomass furnace. *Renew. Energy*. 2017;105:22-29.
30. Cengel MBY. *Thermodynamics: An Engineering Approach*. 7th Edition. New York: McGraw-Hill; 2010. https://www.mheducation.com/highered/product/thermodynamics-engineeringapproach-cengel-boles/M9781259822674.html
31. Velraj R, Seeniraj RV, Hafner B, Faber C, Schwarzer K. Experimental analysis and numerical modelling of inward solidification on a finned vertical tube for a latent heat storage unit. *Sol. Energy*. 1997;60(5):281-290.
32. Enibe S. O., Thermal analysis of a natural circulation solar air heater with phase change material for energy storage, vol. 28, no. 14. 2003.
33. Salazar A. On thermal diffusivity. *Eur. J. Phys.* 2003;24(4):351-358.
34. Saxena A, El-Sebaii AA. A thermodynamic review of solar air heaters. *Renew. Sustain. Energy Rev.* 2015;43:863-890.
35. Mettawee EBS, Assassa GMR. Thermal conductivity enhancement in a latent heat storage system. *Sol. Energy*. 2007;81(7):839-845.

36. Moradi R., Kianifar A., and Wongwises S., "Optimization of a solar air heater with phase change materials: Experimental and numerical study," *Exp. Therm. Fluid Sci.*, vol. 89, no. January, pp. 41–49, 2017.

37. Razak A. A., Majid Z. A. A., Basrawi F., Sharol A. F., Ruslan M. H., and Sopian K., "A performance and technoeconomic study of different geometrical designs of compact single-pass cross-matrix solar air collector with square-tube absorbers," *Sol. Energy*, vol. 178, no. June 2018, pp. 314–330, 2019.

**How to cite this article:** Sharol AF, Abdul Razak A, Abdul Majid ZA, Fudholi A. Experimental study on performance of square tube absorber with phase change material. *Int J Energy Res*. 2019;1-12. https://doi.org/10.1002/er.4971